

Electrostatic Analysis of a Short Accident in Cable Trays for Intelligent Pressure Transmitters

Jaeyul CHOO¹, Hyung Tae KIM¹, Hyun Shin PARK¹ and Choong Heui JEONG¹

¹ Korea Institute of Nuclear Safety, 62 Gwahak-ro, Yuseong-gu, Daejeon, Korea
k728cgy@kins.re.kr, k719kht@kins.re.kr, k394phs@kins.re.kr, chjeong@kins.re.kr

Abstract: We apply the mode-matching method to the electrostatic analysis of shorted enclosed-cable trays that are generally used in industrial facilities such as a nuclear power plant. In mode-matching formulation on potential distribution, we utilize Laplace's equation and superposition principle. After obtaining the modal coefficients from Dirichlet and Neumann boundary conditions, we then derive distributions of potential and electric field, capacitance matrix, effective dielectric constant, and characteristic impedance to evaluate the electromagnetic influence caused by a short accident in the enclosed-cable tray.

Keywords: Enclosed-cable tray, mode-matching method, electromagnetic influence.

1. Introduction

The cable trays have been employed to protect and isolate the power and communication cables from physical and electromagnetic damage and fire attacks in industrial facilities such as a nuclear power plant [1, 2]. Based on the configuration, the cable trays are divided into ladder-type, perforated-type, and solid-bottom-type, etc. To improve the isolation and protection performances, either the enclosed-cable tray or the physical and electromagnetic barrier can be utilized [1, 2].

In this paper, we analyze the electromagnetic influence from the shorted enclosed-cable trays used for intelligent pressure transmitters in nuclear power plants. We assume that two enclosed-cable trays without connection to the ground are located between both lateral walls with the potential of 0 V and shorted by the inner leaky cables. To derive the distributions of potential and electric field, the capacitance matrix, the effective dielectric constant, and the characteristic impedance in the variation of geometrical parameters, we utilize the mode-matching method [3]. Since the wavelength in the operating frequency of the used power cables is generally large (wavelength of about 5000 km in the frequency of 60 Hz) in comparison with the dimension of the analyzed regions, the validation of our electrostatic analysis is ensured.

Note that this study is extended version of previous researches [4, 5] and the novelty of this research is the estimation of the electromagnetic influence from the shorted enclosed-cable trays. The resulted capacitance matrix generally indicates how much the enclosed-cable trays are influenced from adjacent another tray and lateral walls in a short accident. In addition, the investigated effective dielectric impedance and characteristic

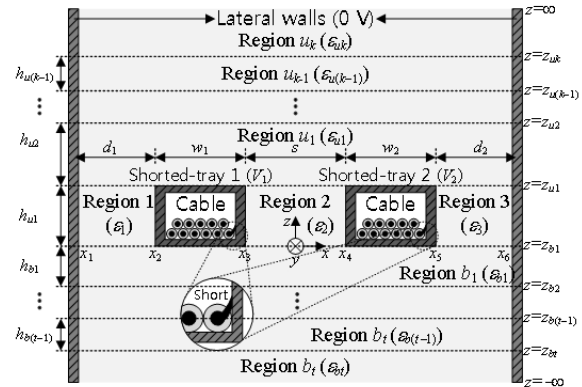


Fig. 1. Cross section of the shorted enclosed-cable trays in the multilayer dielectrics.

impedance provide the useful information for scattering analysis in the short accident of enclosed-cable trays. In what follows, we show a brief mode-matching formulation on the potential distribution and boundary conditions for simultaneous equations

2. Mode-matching Formulation

Fig. 1 illustrates a cross section of two enclosed-cable trays surrounded by multilayer dielectrics with the lateral conducting walls of 0 V. The potentials V_1 and V_2 are applied to two enclosed-cable trays with the widths w_1 and w_2 , respectively, and the separating distance s . The surrounding dielectrics are specifically divided into three different regions, which are regions u_k with ϵ_{uk} ($k = 1, 2, 3, \dots$) for the upper dielectrics, regions b_t with ϵ_{bt} ($t = 1, 2, 3, \dots$) for the bottom dielectrics, and regions 1–3 with $\epsilon_1, \epsilon_2,$

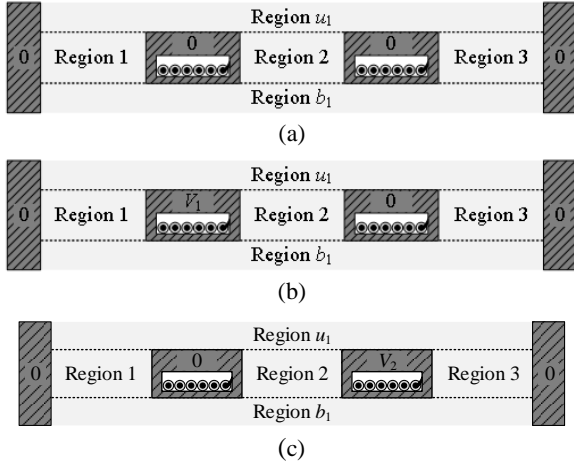


Fig. 2. Equivalent problem based on the superposition principle: (a) case 1, (b) case 2, and (c) case 3.

and ε_3 for the dielectrics adjacent to two enclosed-cable trays. The lateral walls stand apart from the closed-cable trays with distances d_1 and d_2 . Based on the superposition principle, it is tractable that the original problem is considered the decomposed three problems in Fig. 2 where the potentials on the enclosed-cable trays have (0, 0) in case 1, ($V_1, 0$) in case 2, and (0, V_2) in case 3, respectively [3]. Because the potential in each regions satisfies Laplace's equation [3], the potential in every region is expressed as

$$\Phi_1 = \sum_{n_1=1}^{\infty} \sin(m_1(x-x_1))f_1(z) + \frac{V_1}{d_1}(x-x_1) \quad (1)$$

$$\Phi_2 = \sum_{n_2=1}^{\infty} \sin(m_2(x-x_3))f_2(z) + \frac{V_2-V_1}{s}(x-x_3) + V_1 \quad (2)$$

$$\Phi_3 = \sum_{n_3=1}^{\infty} \sin(m_3(x-x_5))f_3(z) - \frac{V_2}{d_2}(x-x_6) \quad (3)$$

$$\Phi_{uk, bt} = \sum_{n_{uk}, n_{bt}=1}^{\infty} \sin(m_{uk, bt}(x-x_1))f_{uk, bt}(z) \quad (4)$$

where $m_1 = n_1\pi / d_1$, $m_2 = n_2\pi / s$, $m_3 = n_3\pi / d_2$, $m_{uk} = n_{uk}\pi / (x_6 - x_1)$, $m_{bt} = n_{bt}\pi / (x_6 - x_1)$ ($k = t = 1, 2, 3, \dots$), and

$$f_{\alpha}(z) = \begin{cases} A_{\alpha}e^{-m_{\alpha}z}, & \text{when } \alpha = uk_{max} \\ B_{\alpha}e^{m_{\alpha}z}, & \text{when } \alpha = bt_{max} \\ A_{\alpha}e^{-m_{\alpha}z} + B_{\alpha}e^{m_{\alpha}z}, & \text{otherwise} \end{cases} \quad (5)$$

Herein k_{max} and t_{max} are the maximum k and t , respectively.

To determine the unknown modal coefficients A_{α} and B_{α} in (5), the Dirichlet conditions for the continuity of potentials at $z = z_{u1}$ and $z = z_{uk}$ yield (6) and (7), respectively.

$$\begin{aligned} & \frac{x_1-x_6}{2} \sum_{n_{u1}=1}^{\infty} f_{u1}(z_{u1})\delta_{m_{u1}p_{u1}} \\ & + \sum_{N=1}^3 \sum_{n_N=1}^{\infty} \left[F(x_{(2N-1)}, x_{2N}, m_N, p_{u1}) f_N(z_{u1}) \right] \\ & = -\frac{V_1}{d_1} g(x_1, x_2) + \frac{V_1-V_2}{b} g(x_3, x_4) - \frac{V_2}{d_2} g(x_6, x_5) \quad (6) \\ & + \frac{V_1-V_2}{p_{u1}} \cos p_{u1}(x_1-x_4) - \frac{V_1}{p_{u1}} \cos p_{u1}(x_1-x_2) \\ & + \frac{V_2}{p_{u1}} \cos p_{u1}(x_1-x_5) \end{aligned}$$

$$\begin{aligned} & \sum_{n_{u(k-1)}=1}^{\infty} F(x_1, x_6, m_{u(k-1)}, p_{uk}) f_{u(k-1)}(z_{uk}) \\ & + \frac{x_1-x_6}{2} \sum_{n_{uk}=1}^{\infty} f_{uk}(z_{uk})\delta_{m_{uk}p_{uk}} = 0 \quad (7) \end{aligned}$$

where $F(a, b, m_{\alpha}, p_{\beta}) = \int_a^b \sin m_{\alpha}(x-a) \sin p_{\beta}(x-x_1) dx$, $g(\beta, \gamma) = \int_{\beta}^{\gamma} (x-\beta) \sin p_{u_1}(x-x_1) dx$, $p_{uk} = q_{uk}\pi / (x_6 - x_1)$, $q_{uk} = 1, 2, \dots$, the maximum n_{uk} , and δ_{mp} is the Kronecker delta.

The Neumann conditions for the continuity of normal derivatives of the potentials at $z = z_{u1}$ and $z = z_{uk}$ yield (8)–(11).

$$\begin{aligned} & \frac{\varepsilon_{u1}}{\varepsilon_1} \sum_{n_{u1}=1}^{\infty} F(x_1, x_2, p_1, m_{u1}) \frac{df_{u1}(z)}{dz} \Big|_{z=z_{u1}} \\ & + \frac{x_1-x_2}{2} \sum_{n_1=1}^{\infty} \frac{df_1(z)}{dz} \Big|_{z=z_{u1}} \delta_{n_1 p_1} = 0 \quad (8) \end{aligned}$$

$$\begin{aligned} & \frac{\varepsilon_{u1}}{\varepsilon_2} \sum_{n_{u1}=1}^{\infty} F(x_3, x_4, p_2, m_{u1}) \frac{df_{u1}(z)}{dz} \Big|_{z=z_{u1}} \\ & + \frac{x_3-x_4}{2} \sum_{n_2=1}^{\infty} \frac{df_2(z)}{dz} \Big|_{z=z_{u1}} \delta_{m_2 p_2} = 0 \quad (9) \end{aligned}$$

$$\begin{aligned} & \frac{\varepsilon_{u1}}{\varepsilon_3} \sum_{n_{u1}=1}^{\infty} F(x_5, x_6, p_3, m_{u1}) \frac{df_{u1}(z)}{dz} \Big|_{z=z_{u1}} \\ & + \frac{x_5-x_6}{2} \sum_{n_3=1}^{\infty} \frac{df_3(z)}{dz} \Big|_{z=z_{u1}} \delta_{m_3 p_3} = 0 \quad (10) \end{aligned}$$

$$\begin{aligned} & \frac{\varepsilon_{u(k-1)}}{\varepsilon_{u_k}} \sum_{n_{u(k-1)}=1}^{\infty} F(x_1, x_6, m_{u(k-1)}, p_{uk}) \frac{df_{u(k-1)}(z)}{dz} \Big|_{z=z_{uk}} \\ & + \frac{x_1-x_6}{2} \sum_{n_{uk}=1}^{\infty} \frac{df_{uk}(z)}{dz} \Big|_{z=z_{uk}} \delta_{m_{uk} p_{uk}} = 0 \quad (11) \end{aligned}$$

For the bottom regions, it is possible to enforce the boundary conditions at $z = z_{b1}$ and $z = z_{bt}$ through the similar procedure. The results from the enforcement of

boundary conditions constitute a set of simultaneous equations for the modal coefficients A_α and B_α . The modal coefficients are calculated efficiently after truncating the infinite series in the simultaneous equations.

3. Computed Results

The numerical computation was performed using Matlab program language. In our computation, it is important to determine the proper truncation number to ensure the convergence of the potential values since the excessive series for the potentials require much computing time. After verifying the fast convergence, we derived the distributions of potential and electric field, capacitance matrix, effective dielectric constant, and characteristic impedance.

2.1. Field Distribution

The time-invariant electric field \vec{E} is derived from the calculated potential as shown in (12).

$$\vec{E} = -\nabla\Phi(x, z) = -\left(\hat{a}_x \frac{\partial\Phi(x, z)}{\partial x} + \hat{a}_z \frac{\partial\Phi(x, z)}{\partial z}\right) \quad (12)$$

Figs. 3 and 4 show the potential distribution and the electric field strength of x -component (E_x) and z -component (E_z) for the shorted enclosed-cable trays with the applied potentials of $V_1 = -1$ and $V_2 = 1$ where the surrounding layers are filled with air ($\epsilon_r = 1$) and the geometry parameters are $w_1 = s = w_2 = 5$ m, $h_{u1} = 1$ m, and $d_1 = d_2 = 10$ m. The electric fields are normalized by the absolute potential difference $|V_2 - V_1|$ between two enclosed-cable trays. Due to the symmetry with respect to y - z plane, both results in Figs. 3 and 4 are seen to be symmetrical distributions.

In Fig. 3, the equivalent potential lines are dense between two enclosed-cable trays (Region 2), which results in strong electric field and electromagnetic coupling. In addition, the equivalent potential lines are tilted to the direction of the lateral walls that indicates the distances d_1 and d_2 are also the important factors influencing on the nearby enclosed-cable trays electromagnetically. Fig. 4 shows the investigation of the electric field strength calculated by (12). As expected, E_x is forceful at the gap between both enclosed-cable trays (Region 2) and between the enclosed-cable trays and the lateral walls (Regions 1 and 3).

In order to evaluate the electromagnetic interference from the lateral walls, we investigated E_x and E_z at $z = 1.5$ m for the enclosed-cable trays with $w_1 = w_2 = 10$ m and $h_{u1} = 0.05$ m when the distance $d_1 (= d_2)$ is 20 m and 400 m as shown in Fig. 5(a) and Fig. 5(b), respectively. For the comparison, the same geometry excluding the lateral shield is computed by the conformal mapping as shown with dashed line [6]. In Fig. 5 the result for $d_1 = d_2 = 400$ m represents that the calculated electric field as a function of the position x shows a favorable agreement with the results derived from the conformal mapping except for

small discrepancies. This results indicate the

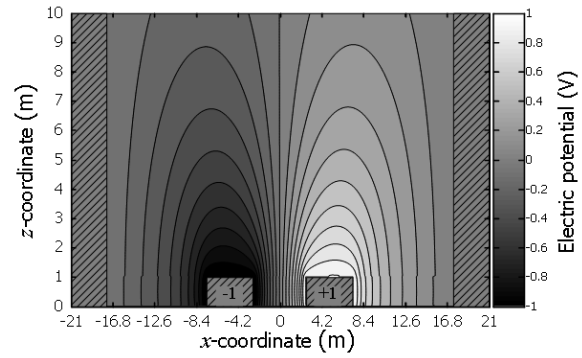
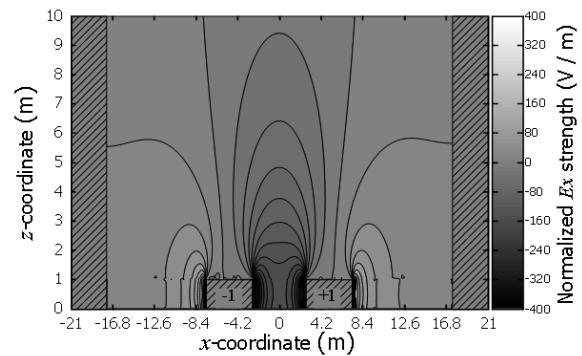
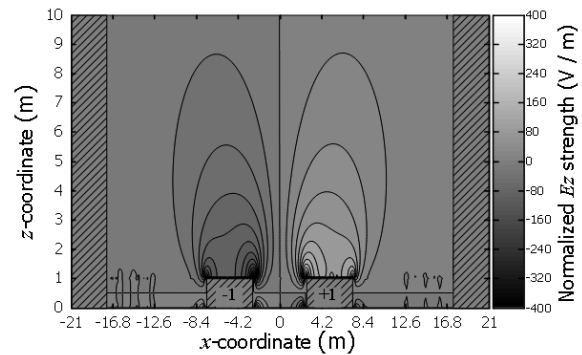


Fig. 3. Potential distribution of enclosed-cable trays surrounded with air ($w_1 = s = w_2 = 5$ m, $h_{u1} = 1$ m, $d_1 = d_2 = 10$ m, $V_1 = -1$, and $V_2 = 1$)



(a)



(b)

Fig. 4. Electric field distribution strength of enclosed-cable trays surrounded with air: (a) x -component (E_x) and (b) z -component (E_z) of electric field strength ($w_1 = s = w_2 = 5$ m, $h_{u1} = 1$ m, $d_1 = d_2 = 10$ m, $V_1 = -1$, and $V_2 = 1$).

electromagnetic coupling from the lateral walls can be neglected in the condition of the proper distances d_1 and d_2 . Note that how much the enclosed-cable trays are electromagnetically coupled with the lateral walls in terms of distances d_1 and d_2 is shown in Section 2.2.

2.2. Capacitance Matrix

Capacitance matrix is generally utilized to evaluate the electrostatic influence on adjacent objects. The capacitance matrix C is defined as [7]

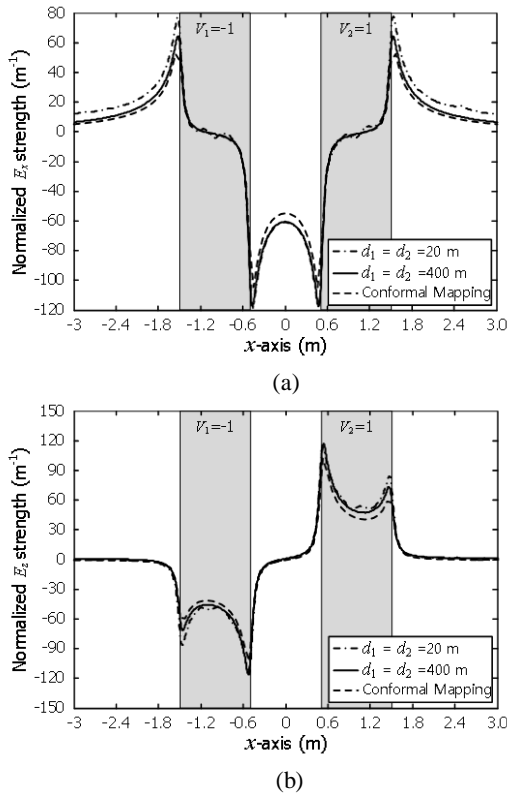


Fig 5. Normalized electric field strength of the symmetric enclosed-cable trays surrounded with air: (a) x -component (E_x), (b) y -component (E_y) ($w_1 = w_2 = s = 10$ m and $h_{u1} = 0.05$ m).

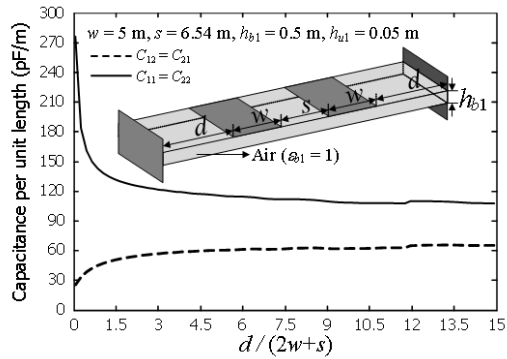


Fig 6. Capacitance matrix of the symmetric enclosed-cable trays surrounded with air when the distance $d_1 (= d_2)$ increases ($w_1 = w_2 = 5$ m, $s = 6.54$ m, $h_{b1} = 0.5$ m, and $h_{u1} = 0.05$ m).

$$[C] = \begin{bmatrix} C_{11} & -C_{12} \\ -C_{21} & C_{22} \end{bmatrix} \quad (13)$$

where each component for the symmetric structure is obtained as

$$C_{11} = C_{22} = \frac{Q_1}{V_1} \Big|_{V_2=0} = \frac{Q_2}{V_2} \Big|_{V_1=0} \quad (14)$$

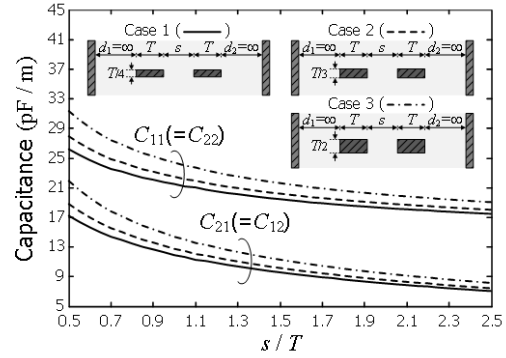


Fig. 7. Capacitances C_{11} and C_{21} of both enclosed-cable trays with vertically parallel placement when the separation distance s varies (case 1: $w_1 = w_2 = T/4$ and $h = T$, case 2: $w_1 = w_2 = T/3$ and $h = T$, and case 3: $w_1 = w_2 = T/2$ and $h = T$).

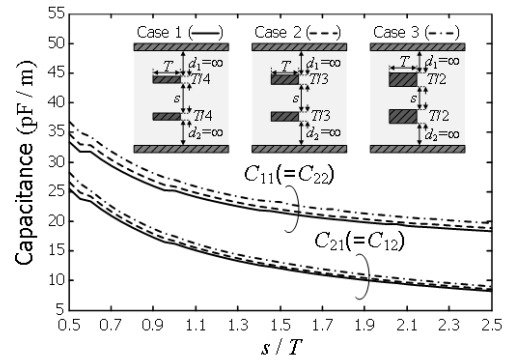


Fig. 8. Capacitances C_{11} and C_{21} of both enclosed-cable trays with vertically parallel placement in free-space when the separation distance s varies (case 1: $w_1 = w_2 = T/4$ and $h = T$, case 2: $w_1 = w_2 = T/3$ and $h = T$, and case 3: $w_1 = w_2 = T/2$ and $h = T$).

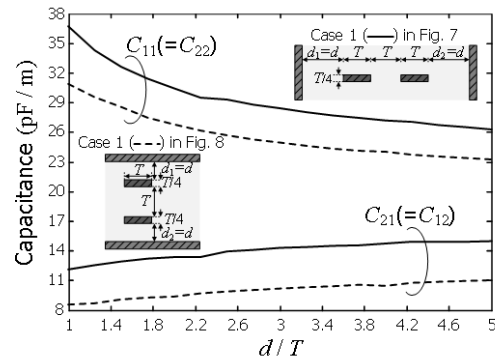


Fig. 9. Capacitances C_{11} and C_{21} of the cases 1 in Figs. 2 and 3 when the distance $d (= d_1 = d_2)$ changes and the separation distance s is T .

$$C_{12} = C_{21} = -\frac{Q_1}{V_2} \Big|_{V_1=0} = -\frac{Q_2}{V_1} \Big|_{V_2=0} \quad (15)$$

Herein both Q_1 and Q_2 represent the charge accumulation per unit length (m) on the shorted enclosed-cable trays 1 and 2, respectively, and are calculated using the integral form of Gauss's law as

$$\oint_{N_{ray\ 1,2}} \bar{D} \cdot d\bar{l} = \epsilon_0 \oint_{N_{ray\ 1,2}} \bar{E} \cdot d\bar{l} = Q_{1,2}. \quad (16)$$

Based on the definition of the capacitance matrix, the capacitance matrix for the same geometry in Fig 6 was investigated when the distance d ($= d_1 = d_2$) changes. Fig. 6 shows the capacitance matrix as a function of $d / (2w + s)$. The C_{11} and C_{12} drastically change when the ratio of $d / (2w + s)$ increases from 0 to about 1. Then the C_{11} and C_{12} converge as the ratio of $d / (2w + s)$ approaches about 15. This investigation would provide the proper distance d from the lateral walls to avoid the electromagnetic coupling between the lateral walls and the enclosed-cable trays.

Figs. 7 and 8 show the capacitance matrices when both shorted enclosed-cable trays in free-space are close to each other horizontally and vertically, respectively. To reveal electrostatic influence only between both shorted enclosed-cable trays excluding that from the lateral walls, the distances d_1 and d_2 were set to be infinite (over 10 times distance of $2T + s$). In Figs. 7 and 8, the capacitances C_{11} and C_{21} are shown to be enlarged when the height of the enclosed-cable trays increases from $T / 4$ (case 1) to $T / 2$ (case 3) as well as the ratio s / T decreases. The investigated results reveal that the separation distance s should be significantly considered for the accumulated enclosed-cable trays to avoid the EMI problems.

In Fig. 9 we investigated the capacitances C_{11} and C_{21} corresponding to the variation in the distance d ($= d_1 = d_2$) in case 1 in Figs. 7 and 8 for evaluating the effect from the lateral walls. In the case 1, the capacitance C_{11} is shown to be increased whereas the capacitance C_{21} is shown to be decreased when the lateral walls approach to the shorted enclosed-cable trays. The deviation between the capacitances C_{11} and C_{21} gives a clue about the favorable placement of the grounded structure to alleviate the undesirable electromagnetic coupling from nearby objects.

2.3. Effective dielectric constants and characteristic impedance

It is possible that the enclosed-cable trays work as a transmission line in low frequency regime. Additionally the effective dielectric constant (ϵ_{eff}) and the characteristic impedance (Z_0) are important characteristics for the scattering analysis of enclosed-cable trays within multiple dielectric layers. We thus derived the effective dielectric constant and the characteristic impedance of the enclosed-cable trays in multiple dielectrics as

$$\epsilon_{eff} = C / C_{wo} \quad (17)$$

$$Z_0 = 1 / c \sqrt{CC_{wo}} \quad (18)$$

where C is the total line capacitance of enclosed-cable tray, C_{wo} is the total line capacitance without dielectric layers, and c is the speed of light in free space ($= 3 \times 10^8$ m / s).

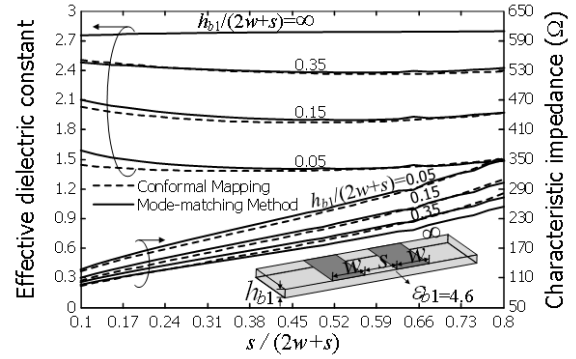


Fig. 10 Effective dielectric constant and characteristic impedance of the shorted enclosed-cable trays on a single layer dielectric with $\epsilon_{b1} = 4.6$.

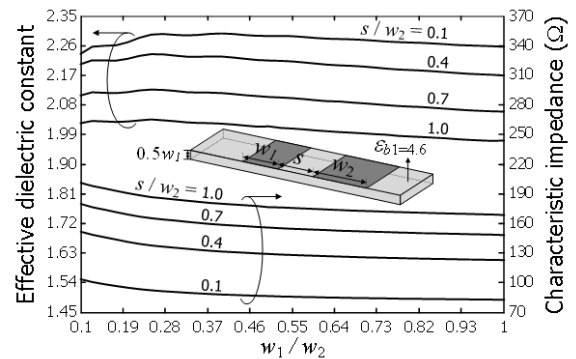


Fig. 11. Effective dielectric constant and characteristic impedance of asymmetric enclosed-cable trays on a single layer dielectric with $h_{u2} = 0.5 w_1$ and $\epsilon_{b1} = 4.6$.

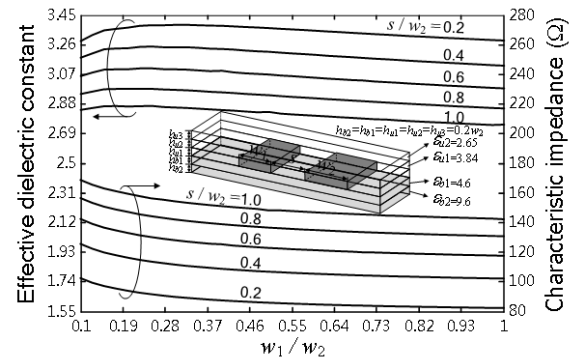


Fig. 12. Effective dielectric constant and characteristic impedance of asymmetric enclosed-cable trays on four layer dielectrics with $h_{b2} = h_{b1} = h_{u1} = h_{u2} = 0.2 w_2$, $\epsilon_{b2} = 2.65$, $\epsilon_{u1} = 3.84$, $\epsilon_{b1} = 4.6$, $\epsilon_{u2} = 2.65$.

Fig. 10 presents the computed effective dielectric constants and characteristic impedances for symmetric enclosed-cable trays ($w_1 = w_2 = w$) on a single layer dielectric with $\epsilon_{b1} = 4.6$. The results are illustrated as a function of $s / (2w + s)$ for several $h_{b1} / (2w + s)$, and they are compared to the results of the conformal mapping technique [8]. The results show a favorable agreement with the conformal mapping technique. The small discrepancies are attributed to the considered thickness h_{u1} of enclosed-cable trays in our approach. The

characteristic impedance is proportional to $s / (2w + s)$, which decreases as $h_{b1} / (2w + s)$ increases. It is seen that the effective dielectric constant increases as the $h_{b1} / (2w + s)$ grows whereas the change in $s / (2w + s)$ has little effect on the effective dielectric constant.

Figs. 11 and 12 illustrate the calculated effective dielectric constants and the characteristic impedances for the asymmetric enclosed-cable trays surrounded with a single layer dielectric and four layers dielectric. The results are shown as a function of w_1 / w_2 for several s / w_2 . As the ratio of the distance to the width (s / w_2) grows, the characteristic impedance increases while the effective dielectric constant decreases. As w_1 / w_2 increases from 0.1 to 1 (in symmetric enclosed-cable trays), the characteristic impedance is shown to gradually decrease while the effective dielectric constant slightly grows and then slowly diminishes, as seen in Figs. 11 and 12. Note that there is no limitation for the number of dielectric layers surrounding the enclosed-cable trays in our approach.

5. Conclusions

The mode-matching method was applied to the electrostatic analysis of the shorted enclosed-cable trays within multiple dielectric layers in nuclear power plants. The mathematical expressions with the unknown modal coefficients for potential distribution were formulated based on Laplace's equation and superposition principle. The modal coefficients with the proper truncation number were then determined from the Dirichlet and Neumann boundary conditions. Using the obtained modal coefficients, we investigated the potential and electric field distributions, the capacitance matrix, the effective dielectric constant, and characteristic impedance varying the placement of the shorted cable trays and the lateral walls as well as the properties of dielectric layers. The investigated results provide the useful information to avoid EMI problems in nuclear power plants.

6. Acknowledge

This work was supported by the Korea Institute of Nuclear Safety under the project 'Development of Proof Test Model and Safety Evaluation Techniques for the Regulation of Digital I&C Systems used in NPPs' (no. 1305003-0315-SB130).

7. References

- [1] M. J. A. M. v. Helvoort, "Grounding structures for the EMC-protection of cabling and wiring", Eindhoven University Eindhoven, Eindhoven, Netherland, 1995.
- [2] *IEEE Standard Criteria for Independence of Class 1E Equipment and Circuits*, IEEE Standard 384, 2008.
- [3] H. J. Eom, "Electromagnetic Wave Theory for Boundary-value Problems", Springer Verlag, Berlin, Germany, 2004.
- [4] J. Choo, S. Y. Jeong, H. T. Kim, Y. J. Yu, H. S. Park, and C.H. Jeong, "Electrostatic analysis of a short accident in cable trays for intelligent pressure transmitters," in *9th International Conference on Electrical and Electronics Engineering*, Bursa,, 2015, pp. 289–293

- [5] J. Choo, C. Cho, and J. Choo, "Simple quasi-static analysis for coplanar stripline within multilayer dielectrics", *IEICE Electron. Express*, vol. 12, no. 17, pp. 1–8
- [6] C. M. Kim and R. V. Ramaswamy, "Overlap integral factors in integrated optic modulators and switches," *J. lightw. Technol.*, vol. 7, no. 7, pp. 1063–1070, Jul. 1989.
- [7] C. Wei, R. F. Harrington, J. R. Mautz, and T. K. Sarkar, "Multiconductor transmission lines in multilayered dielectric media," *IEEE Trans. Microw. Theory Tech.*, vol. 32, no. 4, pp. 439–450, Apr. 1984.
- [8] G. Chione and C. Naldi, "Analytical formulas for coplanar lines in hybrid and monolithic MICs," *Electron. Lett.*, vol. 20, no. 4, pp. 179–181, Feb. 1984.



Jaeyul Choo received the B.S. and M.S. degrees in electronic and electrical engineering from Hongik University, Seoul, Korea, in 2004 and 2006, respectively, and the Ph.D. degree in electrical engineering from the Korea Advanced Institute of Science and Technology, Daejeon, Korea, in 2014. He was an Associate Research Engineer with the Central Research and Development Center, LS Industrial Systems Company, Ltd., Anyang, Korea, from 2006 to 2010. In 2014, he joined the Korea Institute of Nuclear Safety, Daejeon. His current research interests include the design of tag and reader antennas for RFID, the electrical analysis for flip-chip bonding package, and the electromagnetic field analyses of vias, transmission lines, and scattering structure for dealing with electromagnetic interference problems.



Hyungtae Kim received the B.S. degrees in electronic engineering from Pusan National University, Busan, Korea, in 1999 and the M.S. degree in Information Technology from the Pohang University of Science and Technology, Pohang, Korea, in 2001. He was an Junior Research Engineer with the System Research Center, LG Innotek Company, Ltd., Yongin, Korea, from 2001 to 2004. He was an Senior Research Engineer with the Mobile Communications R&D Center, LG Electronics Company, Ltd., Seoul, Korea, from 2004 to 2007. He works for the Korea Institute of Nuclear Safety, Daejeon, Korea. His current research interests include the design of instrumentation and control systems of nuclear power plants and the equipment qualification methodology including electromagnetic compatibility.



control systems of nuclear power plants and the equipment qualification methodology including electromagnetic interference.

Hyun Shin Park received the B.S. and M.S. degrees in electrical engineering from Korea University, Seoul, Korea, in 1987 and 1989, respectively, and the Ph.D. degree in electrical engineering from Choongnam National University, Daejeon, Korea, in 2009. He works for the Korea Institute of Nuclear Safety, Daejeon, Korea. His current research interests include the design of instrumentation and



Energy Research Institute, Daejeon, from 1987 to 1990. In 1990, he joined the Korea Institute of Nuclear Safety, Daejeon. His current research interests include the electromagnetic field analyses of vias, transmission lines, and scattering structure for dealing with electromagnetic interference problems.

Choong Heui Jeong received the B.S. degrees in electronic engineering from Ajou University, Suwon, Korea, in 1984, and received the M.S. degrees and completed the doctoral course in computer engineering from Choongnam University, Daejeon, Korea, in 2002 and 2006, respectively. He had been a junior Researcher in the 3rd Inspection Office of Nuclear Safety Center, an attached organization of Korea Atomic